Data-adaptive unfolding of nuclear excitation spectra: a time-series approach

Data-adaptive unfolding of nuclear excitation spectra: a time-series approach

G Torres Vargas[1], R Fossion[2,3], V Velázquez[4], J C López Vieyra[5]

[1] Posgrado en Ciencias Físicas, Universidad Nacional Autónoma de México, 04510 México, D.F., Mexico
[2] Instituto Nacional de Geriatría, Periférico Sur No. 2767, 10200 México D.F., Mexico
[3] Centro de Ciencias de la Complejidad (C3), Universidad Nacional Autónoma de México, 04510 México, D.F., Mexico
[4] Facultad de Ciencias, Universidad Nacional Autónoma de México, 04510 México, D.F., Mexico
[5] Instituto de Ciencias Nucleares, Universidad Nacional Autónoma de México, 04510 México, D.F., Mexico

E-mail: `fossion@nucleares.unam.mx`

Abstract. A common problem in the statistical characterization of the excitation spectrum of quantum systems is the adequate separation of global system-dependent properties from the local fluctuations that are universal. In this process, called *unfolding*, the functional form to describe the global behaviour is often imposed externally on the data and can introduce arbitrarities in the statistical results. In this contribution, we show that a quantum excitation spectrum can readily be interpreted as a time series, before any previous unfolding. An advantage of the time-series approach is that specialized methods such as Singular Spectrum Analysis (SSA) can be used to perform the unfolding procedure in a data-adaptive way. We will show how SSA separates the components that describe the global properties from the components that describe the local fluctuations. The partial variances, associated with the fluctuations, follow a definite power law that distinguishes between soft and rigid excitation spectra. The data-adaptive fluctuation and trend components can be used to reconstruct customary fluctuation measures without ambiguities or artifacts introduced by an arbitrary unfolding, and also define the global level density of the excitation spectrum. The method is applied to nuclear shell-model calculations for ^{48}Ca, using a realistic force and Two-Body Random Ensemble (TBRE) interactions. We show that the statistical results are very robust against a variation in the parameters of the SSA method.

1. Introduction

According to the conjectures of Berry-Tabor [1] and Bohigas-Giannoni-Schmit [2], level fluctuations of the excitation spectra of dynamical quantum systems obey universal laws that can be described with Random Matrix Theory (RMT). These universal laws do not depend on the specific details of the particular system, and instead only depend on the underlying physical symmetries [3]; more specifically, excitation spectra of quantum systems with time-reversal symmetry are predicted to obey the statistics of the Gaussian Orthogonal Ensemble (GOE), systems without time-reversal symmetry follow the predictions of the Gaussian Unitary Ensemble (GUE), systems with time-reversal symmetry but no rotational symmetry follow the Gaussian

Symplectic Ensemble (GSE), whereas integrable systems obey Poisson statistics (sometimes also referred to as the Gaussian Diagonal Ensemble or GDE [4]). The BGS conjecture has been confirmed in a wide variety of quantum systems, from two-dimensional systems such as quantum billiards and microwave cavities, up to many-body systems such as atoms, quantum dots, hadrons, and atomic nuclei (see [5, 6, 7, 8, 9, 10] for recent reviews). Excitation spectra of all these systems have in common that the density of states (DOS) $\rho(E)$ grows rapidly with excitation energy E because of pure combinatorial reasons, whereas the dynamics of the system (shape of mean field and/or presence of residual interactions) introduces local fluctuations around this global behaviour [11]. Thus, a statistical study of the level fluctuations of a quantum excitation spectrum offers a basic tool to elucidate the system's underlying dynamics.

Of great importance and prior to any statistical study, is the *unfolding procedure* that serves two purposes:

- to separate the system-dependent global level-density behaviour $\overline{\rho}(E)$ from the universal local fluctuations $\widetilde{\rho}(E) = \rho(E) - \overline{\rho}(E)$
- to rescale the level-spacing fluctuations to unit mean spacing so that the statistics of different systems can be compared with RMT predictions

In the traditional approach to the unfolding procedure (see e.g. [12]), a mapping of the sequence of actual energy levels $\{E(i), i = 1 \dots N\}$, into dimensionless levels $\varepsilon(i)$,

$$E(i) \to \varepsilon(i) \equiv \overline{\mathcal{N}}\left[E(i)\right] = \int_{-\infty}^{E(i)} \overline{\rho}(E')dE', \tag{1}$$

realizes this process. Here, $\overline{\mathcal{N}}\left[E\right]$ is a smooth approximation to the accumulated or integrated density function (IDOS) $\mathcal{N}\left[E(i)\right] = \sum_{i=1}^{N} \theta\left(E - E(i)\right)$, where θ is the Heaviside step function. $\mathcal{N}\left[E(i)\right]$ counts the exact number of levels i up to excitation energy $E(i)$, and increases by one unit as the energy E passes a (non-degenerate) eigenvalue $E(i)$ [6, 7, 13]. The unfolding procedure is straightforward if a theoretical prediction for the average level density $\overline{\rho}(E)$ is available, e.g. the Weyl formula in the case of quantum billiards [9], the semi-circular distribution in the case of GOE, and the normal distribution in the Poisson case [3]. However, an analytical form for $\overline{\rho}(E)$ is usually only valid in the asymptotic limit for spectra with a very large number of levels $N \to \infty$ [8] and often is not known [7]. In those cases, a local unfolding can be applied, which can only be used to study short-range correlations [14]. Another approach, advantageous especially when the excitation spectrum contains relatively few levels, is to model the smooth behaviour of IDOS $\overline{\mathcal{N}}\left[E\right]$ rather than the global behaviour of DOS $\overline{\rho}(E)$, because the histogram representation of the latter depends on the width of the bins chosen [7]. Often, $\overline{\mathcal{N}}\left[E\right]$ is approximated by imposing a fit with a polynomial in energy E. However, the degree of the polynomial needs to be chosen carefully to avoid artifacts [10, 14]. Literature is unanimous on the fact that performing the unfolding procedure is not always an obvious task (see e.g. [9, 10, 12, 14, 15, 8, 16, 17, 18, 19]).

In [4, 10, 20], it was suggested to interpret the unfolded level fluctuations,

$$\begin{aligned} \widetilde{\mathcal{N}}\left[E(i)\right] &= \mathcal{N}\left[E(i)\right] - \overline{\mathcal{N}}[E(i)] \\ &\equiv -\delta_n = -\sum_{i=1}^{n}\left(s_i - \langle s\rangle\right) = -\left(\varepsilon_n - \varepsilon_1 - n\left\langle s\right\rangle\right) \end{aligned} \tag{2}$$

as a generalized time series. Here $s_i = \varepsilon_i - \varepsilon_{i-1}$ are the unfolded and rescaled level spacings with $\langle s\rangle = 1$. In [21], it was shown that the definitions $\widetilde{\mathcal{N}}\left[E(i)\right]$ and δ_n are equivalent. An

advantage of the time-series approach is that now techniques from signal analysis from classical physics, such as Fourier spectral analysis, become available to study the quantum level fluctuations. Level fluctuations for GOE, GUE and GSE systems were found to behave as $1/f$ noise, whereas level fluctuations from systems that obey Poisson statistics behave as Brownian $1/f^2$ noise. Particular cases intermediate between Poisson and GOE behave as $1/f^\beta$ noise with $1 < \beta < 2$ [10, 20]. In [22, 23], use was made of the time-series interpretation of the unfolded level-fluctuations $\widetilde{\mathcal{N}}[E(i)]$ of eq. (2) to apply data-adaptive techniques from signal analysis to detect and correct for spurious correlations introduced by the polynomial unfolding.

The purpose of the present contribution is to show that data-adaptive techniques from signal analysis can be used not only to characterize the statistics of the unfolded level fluctuations, but to perform the very unfolding process itself. In this way, the global spectral properties and the local fluctuations are derived intrinsically, without the need to impose a user-predefined functional on the data. In fact, a similar problem in the context of time-series analysis is how to define the trend of a nonstationary time series. In a recent article [24], the importance of defining the trend in a data-adaptive way has been pointed out. Often, a requirement for the application of techniques from signal analysis is that the time series to be analyzed must be equally spaced. For this reason, we will focus on the sequence of excitation energies $\{E(i), i = 1 \dots N\}$, which is regularly sampled at steps $\Delta i = 1$, in contrast to the IDOS sequence $\mathcal{N}[E(i)]$ of eq. (1), which is not regularly sampled, $\Delta E \neq$ const, see Fig. 1. Our main point is that the sequence of actual energy levels $E(i)$ can readily be interpreted as a generalized time series, albeit with a monotonously rising behaviour. In the following, we will show that the data-adaptive technique of Singular Spectrum Analysis (SSA) [25, 26] decomposes the energy sequence $E(i)$ in a self-consistent way into a global part and a locally fluctuating part, i.e.

$$E(i) = \overline{E}(i) + \widetilde{E}(i), \tag{3}$$

which permits to extract unequivocal conclusions about the fluctuating part without the need for any previous and possibly arbitrary (local or polynomial) unfolding, as shown below.

2. Time-series analysis with Singular Spectrum Analysis (SSA)

2.1. The SSA technique

In contrast to some other data-adaptive techniques, SSA is easy to implement, can be applied to relatively short and also monotonous time series, with as only restriction that the time series needs to be regularly sampled, see Fig. 1. SSA time-series decomposition has been successfully applied in many different fields such as climatology, geology and physiology [25, 26], and the technique will be briefly discussed here. Let $f(i)$ with $i = 1, 2, \dots N$ be a discrete time series. Using the lagged vectors $X_j = (f(j), f(j+1), \dots f(j+L-1))$ with *embedding dimension* $L \leq N/2$, a so-called *trajectory matrix* $\mathbf{X} = [X_1, X_2 \dots X_K]^T$ is constructed, with $K = N - L + 1$. L is one of the few parameters of the SSA method, and we will show that in the application presented in this contribution the statistical results are very robust against a variation in the parameters. Singular Value Decomposition (SVD) is applied to $\mathbf{X}$, to identify the most meaningful basis to re-express the data. SVD decomposes $\mathbf{X}$ in a unique and exact way as a matrix product and a matrix sum $\mathbf{X} = \mathbf{U}\mathbf{\Sigma}\mathbf{V}^T = \sum_{k=1}^{r} \sigma_k \mathbf{X}_k$, where r is the rank of matrix $\mathbf{X}$ and $r \leq \min[K, L]$. The $K \times L$-dimensional matrix $\mathbf{\Sigma}$ contains only diagonal elements which are the ordered weights or singular values $\sigma_1 \geq \sigma_2 \geq \ldots \geq \sigma_r$, and $\mathbf{X}_k = \vec{u}_k \vec{v}_k^T \equiv \vec{u}_k \otimes \vec{v}_k$ are rank-1 elementary matrices. The columns $\vec{u}_k$ of the $K \times L$-dimensional matrix $\mathbf{U}$ are the new basis vectors for the time series, and the columns $\vec{v}_k$ of the $L \times L$-dimensional matrix $\mathbf{V}$ are the

associated projection coefficients. The vectors $\vec{u}_k$ can be interpreted as well as the eigenvectors of the covariance matrix $\mathbf{S}_1 = \mathbf{X} \cdot \mathbf{X}^T$ and can serve as data-adaptive filters for the time series; the associated projection coefficients can then be calculated as $\vec{v}_k = \mathbf{X}^T \cdot \vec{u}_k/\sigma_k$. Alternatively, the vectors $\vec{v}_k$ can be interpreted as the eigenvectors of the covariance matrix $S_2 = \mathbf{X}^T \cdot \mathbf{X}$, and when they are taken as data-adaptive filters then the corresponding coefficients are $\vec{u}_k = \vec{v}_k \cdot \mathbf{X}^T/\sigma_k$. The covariance matrices $\mathbf{S}_1$ and $\mathbf{S}_2$ share the same eigenvalues λ_k. The partial variance of the original time series $f(i)$ in direction $\vec{v}_k$ is given by $\lambda_k = \sigma_k^2$, whereas $\sum_{k=1}^{L} \lambda_k$ gives the total variance. Hankelization or diagonal averaging of the elementary matrix $\mathbf{X}_k$ generates the reconstructed component $g_k(i)$ and the original time series can be written exactly as the weighted sum of reconstructed components, see [25, 26],

$$f(i) = \sum_{k=1}^{L} \sigma_k g_k(i). \tag{4}$$

2.2. Trend and fluctuation analysis with SSA

SSA is a modern approach to trend extraction from a time series [27]. If the trend dominates over the fluctuations, and thus is responsible for the major part of the variance of the time series, then the trend components $g_k(i)$ are distinguished by their large partial variances λ_k [26, 27]. This is clearly the case for the energy sequence $E(i)$ or IDOS $\mathcal{N}[E]$ of a quantum excitation spectrum, which are monotonously rising functions, and often fluctuations are orders of magnitude smaller than the global behaviour, see Fig. 1 and 2. In the context of SSA, *detrending* of a time series corresponds with the separation of non-oscillating components with dominant partial variances from oscillating components with much smaller partial variances. Apart from the trend, SSA can also analyze the oscillatory components of a time series. In [19], the covariance matrices S of an ensemble of already unfolded excitation spectra corresponding to GOE and Poisson statistics were calculated. The resulting eigenvectors U_k were interpreted as *normal modes* for the level fluctuations. The diagram of ordered partial variances, or so-called *scree diagram*, was used to study the rigidity of the fluctuations. The scree diagram follows a power law,

$$\lambda_k \sim 1/k^{\gamma}, \tag{5}$$

with $\gamma \approx 1$ in the rigid case (GOE) and $\gamma \approx 2$ in the soft case (Poisson). Normal-mode analysis is related to Fourier spectral analysis: in the case of fractional Brownian motion (fBm) [28] for which the Fourier power spectrum behaves as a power law $P(f) \sim 1/f^{\beta}$, one finds a corresponding power law for the scree diagram of the form of eq. (5), with similar exponents $\beta \approx \gamma$. These results are thus in correspondence with results of refs. [4, 10, 20, 21] on the Fourier spectral analysis of time series of already unfolded quantum energy levels $\widetilde{N}[E(i)]$ (see eq. (2)) for systems obeying Poison statistics (Brownian $1/f^2$ noise) and GOE, GUE and GSE systems ($1/f$ noise).

3. Data-adaptive unfolding of quantum excitation spectra

3.1. Detrending step

When SSA is applied to a quantum excitation spectrum, then according to eq. (4), the energy sequence $\{E(i), i = 1 \ldots N\}$ can be decomposed as $E(i) = \sum_{k=1}^{L} \sigma_k g_k(i)$. The trend part,

$$\overline{E}(i) = \sum_{k=1}^{n_T} \sigma_k g_k(i), \tag{6}$$

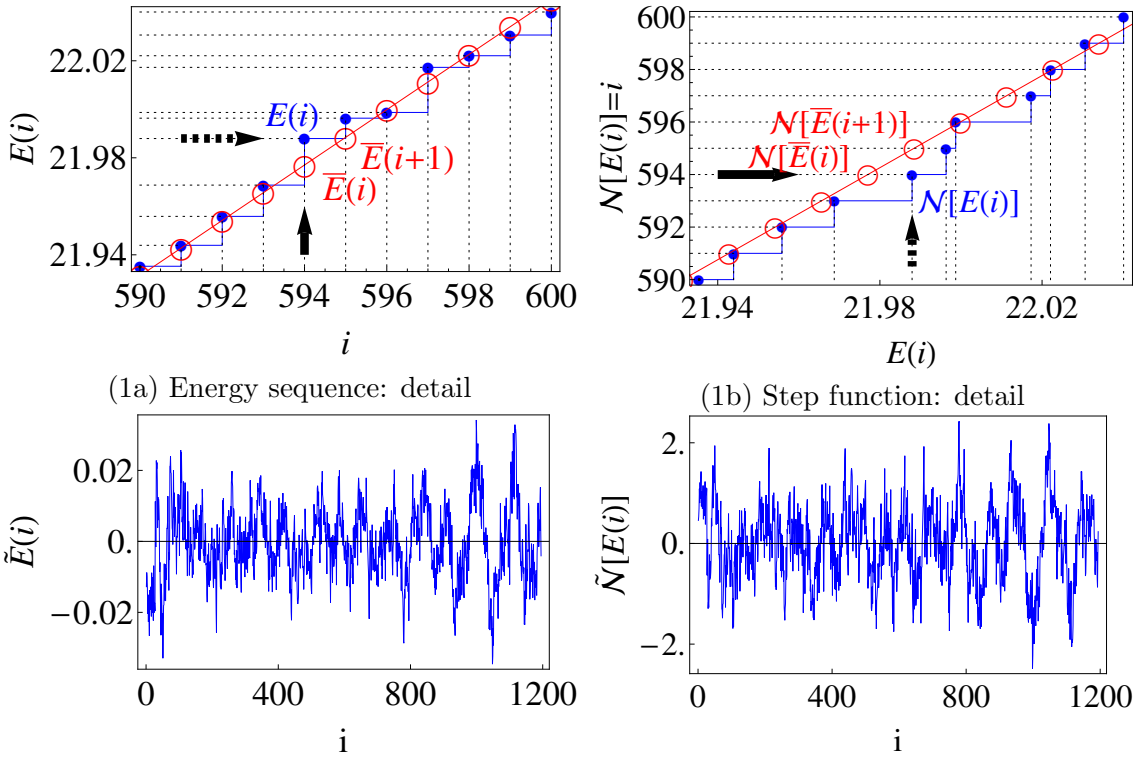

(1a) Energy sequence: detail (1b) Step function: detail

(2a) Energy sequence: fluctuations (2b) Step function: fluctuations

Figure 1. Detail of the energy sequence $E(i)$ (panel (1a)) and integrated density of states (IDOS) $\mathcal{N}[E(i)]$ (panel (1b)) for a realistic shell-model calculation of the $J^\pi = 4^+$ subspectrum of ^{48}Ca consisting of $N = 1195$ energy levels (blue filled circles). Details of the shell-model calculation are given in Sect. 4. $E(i)$ and $\mathcal{N}[E(i)]$ are compared with their respective trends (red open circles), $\overline{E}(i)$ (eq. (6)) and $\mathcal{N}[\overline{E}(i)]$ (eq. (8)), determined data-adaptively with SSA. $E(i)$ is regularly spaced, whereas $\mathcal{N}[E(i)]$ is not regularly spaced (dotted lines indicate the coordinates of the actual excitation energies). A deviation from the trend in the horizontal direction is necessarily accompanied with a deviation in the vertical direction, as indicated by the arrows for a particular fluctuation at $i = 594$. Thus, apart from obvious differences in sign and scale, energy-sequence fluctuations $\widetilde{E}(i) = E(i) - \overline{E}(i)$ (panel (2a) and eqs. (3) and (7)) and IDOS fluctuations $\widetilde{\mathcal{N}}[E(i)] = \mathcal{N}[E(i)] - \mathcal{N}^{\mathrm{intrpl}}_{E(i)}[\overline{E}(i)]$ (panel (2b) and eq. (9)) are statistically equivalent. Note that the fluctuations $\widetilde{E}(i)$ and $\widetilde{\mathcal{N}}[E(i)]$ are orders of magnitude smaller than the global behaviour of $E(i)$ and $\mathcal{N}[E(i)]$, respectively.

is separated from the fluctuation part,

$$\widetilde{E}(i) = \sum_{k=n_T+1}^{L} \sigma_k g_k(i) \tag{7}$$

and the number of components n_T to be included into the trend is defined in a data-adaptive way, by identifying the dominant partial variances $\lambda_k = \sigma_k^2$ with $k = 1 \ldots n_T$, see Fig. 3. This detrending corresponds to the first step of the unfolding procedure. Already during the detrending step, the power law $\lambda_k \sim 1/k^\gamma$ of eq. (5) of the fluctuation part of the scree diagram distinguishes between soft ($\gamma \approx 2$) and rigid ($\gamma \approx 1$) spectra, see Fig. 3. If desired, the trend part $\overline{E}(i)$ can be used to calculate the global DOS $\overline{\rho}(E) = \rho(\overline{E})$ of the quantum excitation

spectrum, see Fig. 2. On the other hand, specialized techniques from signal analysis can be applied to the fluctuation part $\widetilde{E}(i)$ to further characterize the fluctuation statistics. An advantage of using time-series based fluctuation measures, such as normal-mode analysis [19], Fourier spectral analysis [4, 18] or Detrended Fluctuation Analysis (DFA) [18, 29], is that $\widetilde{E}(i)$ does not need to be rescaled prior to analysis, because in the case of power-law behaviour the scale is absorbed in the offset, whereas information on the correlations is codified in the exponent of the power law, see Fig. 3 and 4 (panels (1)). In principle, if one could unfold both the step function $\mathcal{N}[E(i)]$ and the energy sequence $E(i)$ of a given excitation spectrum without ambiguities, the fluctuations obtained, $\widetilde{N}[E(i)]$ and $\widetilde{E}(i)$, respectively, would be statistically similar, see Fig. 1. The most important difference being that the former fluctuations are detrended and rescaled, whereas the latter fluctuations are only detrended.

3.2. Rescaling step

Some of the traditional spectral fluctuation measures require an explicit prior rescaling of the level fluctuations, as is the case of the short-range correlation measure of the Nearest Neighbour Spacing (NNS) distribution, and the long-range correlation measure of the Δ_3 statistic [3]. Such rescaling is traditionally achieved by projecting the excitation energies over the smooth trend $\overline{\mathcal{N}}[E(i)]$ fitted to the integrated density function (IDOS) $\mathcal{N}[E(i)]$, see eq. (1). In the present case, this smooth trend is instead given data-adaptively by integrating the SSA energy trend $\overline{E}(i)$, i.e. by the step function $\mathcal{N}[\overline{E}]$. For the projection, we then get,

$$E(i) \rightarrow \eta(i) = \mathcal{N}^{\mathrm{intrpl}}_{E(i)}[\overline{E}(i)] = \mathcal{N}[\overline{E}(i)] + \frac{E(i) - \overline{E}(i)}{\overline{E}(i+1) - \overline{E}(i)}, \tag{8}$$

where a linear interpolation has been used in between trend values $\mathcal{N}[\overline{E}(i)]$ and $\mathcal{N}[\overline{E}(i+1)]$, see Fig. 1. Following the mapping of eq. (8), the detrended and rescaled level fluctuations are given by,

$$\widetilde{\mathcal{N}}[E(i)] = \mathcal{N}[E(i)] - \mathcal{N}^{\mathrm{intrpl}}_{E(i)}[\overline{E}(i)], \tag{9}$$

from which the Δ_3 statistic can be calculated, see Fig. 4 (panels (2)). The corresponding level spacings are given by,

$$s(i) = \eta(i) - \eta(i-1). \tag{10}$$

By construction, the level spacings $s(i)$ are now normalized to unit mean spacing $\langle s \rangle = 1$, as required by the NNS statistic, see Fig. 4 (panels (3)).

4. Results: Application to the excitation spectrum of the atomic nucleus ^{48}Ca

The present unfolding method, based on the SSA time-series data-adaptive technique, is tested for the excitation spectrum of the ^{48}Ca atomic nucleus. Fluctuation studies must be applied to levels with the same quantum numbers; we choose the $J^\pi = 4^+$ subspectrum because it has the largest number of levels. The level fluctuations of ^{48}Ca have been thoroughly studied in literature and have been found to correspond with GOE predictions [10, 18, 22, 30, 31], which permits to verify the validity of the SSA unfolding method. The energy sequence $\{E(i), i = 1 \ldots N\}$ is calculated with a nuclear shell-model code, based on ANTOINE [32]. ^{48}Ca is an obvious choice to study within the nuclear-shell model framework, because an inert ^{40}Ca core can be assumed, and calculations can be carried out in the full neutron fp shell. All figures in this contribution are

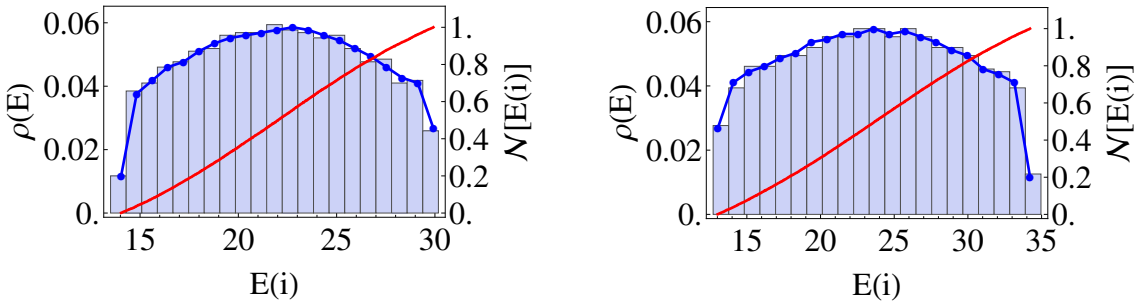

(a) One realization with a realistic calculation (b) One realization of the TBRE ensemble

Figure 2. Density of states (DOS) $\rho(E) = \mathrm{d}\mathcal{N}(E)/\mathrm{d}E = \sum_i \delta(E - E(i))$ [13] (histogram), compared with the mean DOS $\overline{\rho}(E) = \rho(\overline{E}) = \mathrm{d}\mathcal{N}(\overline{E})/\mathrm{d}E = \sum_i (E - \overline{E}(i))$ calculated data-adaptively with SSA from the trend $\overline{E}(i)$ of eq. (6) (blue line), for the $J^\pi = 4^+$ subspectrum of ^{48}Ca. The integrated density of states (IDOS) $\mathcal{N}(E) = \overline{\mathcal{N}}(E) + \widetilde{\mathcal{N}}(E)$ (red line) is a monotonously rising function, with a dominant global trend $\overline{\mathcal{N}}(E)$. For representational purposes, in these figures, $\mathcal{N}(E)$ has been normalized such that $\mathcal{N}(E_{\max}) = 1$.

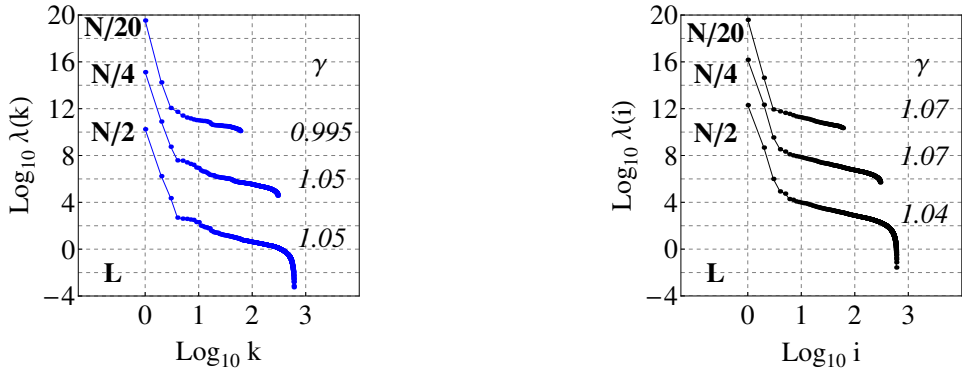

(a) Realistic calculation (b) TBRE ensemble

Figure 3. Scree diagram of ordered partial variances λ_k resulting from the SSA analysis of the energy sequence $\{E(i), i = 1 \ldots N\}$ for the $J^\pi = 4^+$ subspectrum of ^{48}Ca, in case of (a) a single realization of the spectrum using a realistic interaction (blue), and (b) an ensemble mean with $n = 8$ realizations of the spectrum using Two-Body Random Ensemble (TBRE) interactions (black). Details of the calculation are presented in Sect. 4. The largest λ_k with $k = 1, \ldots n_T$ are separated by orders of magnitude from the smaller λ_k and correspond to the trend $\overline{E}(i)$, see eq. (6). The smaller λ_k with $k = (n_T + 1), \ldots L$ correspond to the fluctuations $\widetilde{E}(i)$, see eq. (7), and follow a power law $\lambda(k) \sim 1/k^\gamma$ with exponent $\gamma \approx 1$, see eq. (5), indicating a rigid quantum excitation spectrum. The power law is independent from the embedding dimension L. Shown for $L = N/2, N/4$ ($n_T = 3$) and $N/20$ ($n_T = 2$). The different scree diagrams have been shifted vertically for reasons of comparison.

based on data from this shell-model calculation, for a single realization of the spectrum using a realistic interaction (KB3 [33, 34]) (left panels), and for an ensemble of $n = 8$ realizations using random interactions (TBRE [21, 35]) (right panels). To take into account only the bulk (central part) of the spectrum, 16% of the lower and upper levels have been discarded, and the unfolding is applied to a total of $N = 1195$ levels.

In Fig. 3, the scree diagram of ordered partial variances λ_k is shown for three different choices of

embedding dimension L. It can be seen that in all three cases, the first $n_T = 2$ (for $L = N/20$) or $n_T = 3$ (for $L = N/4, N/2$) largest partial variances λ_k separate from the rest of the eigenvalues (note the double logarithmic scale!). These λ_k with $k = 1, \ldots, n_T$ correspond with the reconstructed components $g_k(i)$ that carry most ($> 99.99\%$) of the variance of the energy sequence $E(i)$, and constitute its monotonous and non-oscillating trend $\overline{E}(i)$, see eq. (6). The smaller eigenvalues λ_k with $k = (n_T + 1), \ldots L$ behave as the power law of eq. (5) with exponent $\gamma \approx 1$, indicating a rigid power spectrum, as expected for the $J^\pi = 4^+$ subspectrum of ^{48}Ca [18]. It is easy to check that the corresponding reconstructed components $g_k(i)$ oscillate with an average frequency proportional to k, and they describe the local level fluctuations $\widetilde{E}(i)$ of eq. (7). It is worth noticing that the power-law exponent γ does not depend on the particular choice of embedding dimension L, and does not depend on the number of trend components n_T either, as long as $n_T \geq 2$ or $n_T \geq 3$, respectively. For very large L ($L \approx N/2$), the decomposition includes a large number of insignificantly small eigenvalues, whereas for very small L ($L \approx N/20$), the range over which the power-law behaviour is observed is reduced. In the present contribution, we use an intermediate choice, namely $L = N/4$ (also recommended in [25]).

In Fig. 2, the DOS $\rho(E)$ is shown for the $J^\pi = 4^+$ subspectrum of ^{48}Ca, in comparison with the global DOS $\overline{\rho}(E)$ as follows from the SSA data-adaptive trend $\overline{E}(i)$ from eq. (6). In the case of atomic nuclei, understanding the level density is very important in order to understand compound nuclear reactions. Two important examples of nuclear reactions are the decay of the giant-dipole resonance in hot nuclei, and the radiative capture of protons, neutrons, $\alpha-$particles, etc., in nucleosynthesis. In order to have predictions in nuclei where no experimental information is available, the global level density $\overline{\rho}(E)$ can be modelled by theory, using e.g. the Bethe formula [36], the binomial distribution [37], or Monte-Carlo shell-model calculations [38]. The SSA defined global level density $\overline{\rho}(E)$ permits to check the adequacy of the predicted level densities for some carefully chosen exerimental test cases where $\rho(E)$ is known.

In Fig. 4 (panels (1)), the Fourier power spectrum of the detrended fluctuation series $\widetilde{E}(i)$ of eq. (7) is presented. Results are shown for $L = N/4$ and for $n_T = 3, 5$ and 10. In all cases, the power spectrum corresponds with $1/f$ noise ($\beta \approx \gamma \approx 1$), indicating a rigid spectrum, independently from the specific choice of the number of trend components n_T. Only the range over which the power law is observed, diminishes when more monotonous or slowly oscillating components are included in the trend (excluded from the fluctuations).

In Fig. 4 (panels (2)), the long-range fluctuations statistic Δ_3 is shown for the detrended and rescaled level fluctuations $\eta(i)$ of eq. (8), and is found to correspond well with the GOE prediction. Results are shown for $L = N/4$ and $n_T = 3, 5$ and 10, and results are found to be very robust against the specific choice of the parameters, with as only difference that the large-scale behaviour of Δ_3 flattens out when more monotonous or slowly oscillating components are included in the trend (excluded from the fluctuations).

In Fig. 4 (panels (3)), the short-range fluctuation statistic of the NNS distribution $P(s)$ is shown for the detrended and rescaled the level spacings $s(i) = \eta(i) - \eta(i-1)$ of eq. (10), and corresponds well with the Wigner surmise $P_W(s) = (\pi s/2) \exp(-\pi s^2/4)$ for GOE. Results are shown for $L = N/4$ and $n_T = 3$, but results are found to be independent from the specific choice of the parameters.

5. Conclusions

We have proposed a method to realize a data-adaptive unfolding of quantum excitation spectra, which avoids the possible ambiguities when the unfolding functional form is imposed externally to the data (e.g. using a polynomial of arbitrary degree). We interpreted the sequence of actual energy levels $\{E(i), i = 1 \dots N\}$ as a generalized time series, and used the data-adaptive SSA method to separate in an unambiguous way the global trend $\overline{E}(i)$ from the local fluctuations $\widetilde{E}(i)$. This first step corresponds with the detrending part of the unfolding procedure. The statistical results are very robust against a variation in the two parameters of the method (embedding dimension L and number of trend components n_T). The partial variances, associated to the fluctuations, follow a power law that distinguishes between soft and rigid excitation spectra. If desired, the data-adaptive trend components $\overline{E}(i)$ can be used to calculate the global level density behaviour, and specialized techniques from signal analysis can be applied to the data-adaptive fluctuation components $\widetilde{E}(i)$ to further specify the fluctuation statistics. Also the rescaling step of the unfolding procedure can be carried out in a self-consistent way, after which traditional fluctuation measures such as the Nearest-Neighbour Spacing (NNS) distribution and Δ_3 can be calculated without ambiguities. We tested the present data-adaptive unfolding method for the $J^\pi = 4^+$ excitation subspectrum of the ^{48}Ca atomic nucleus, and our results are in correspondence with previous results in literature. This also illustrates the fact that the fluctuations in the excitation energies $\widetilde{E}(i)$ (considered in the present contribution) are statistically equivalent to the fluctuations $\widetilde{\mathcal{N}}[E(i)]$ of the integrated density function (IDOS) (considered traditionally). In a forthcoming publication, we will show that the proposed unfolding method is general enough to apply to the excitation spectra of other quantum systems, and also to the eigenspectra of random matrices in various applications in quantum and classical physics [39].

We acknowledge financial support from CONACYT (grants CB-2011-01-167441, CB-2010-01-155663, I010/266/2011/C-410-11 and grant 351103 from the Red Temática Envejecimiento, Salud y Desarrollo Social), PAPIIT-DGAPA (grant IN114411), the European Commission (project FP7-PEOPLE-2009-IRSES-247541-MATSIQEL) and the Instituto Nacional de Geriatría (project DI-PI-002/2012). The authors wish to thank Dr. A. Frank and collaborators for fruitful discussions.

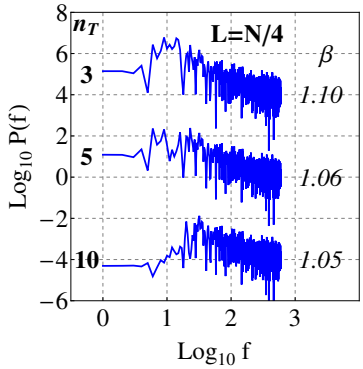

(1a) Realistic calculation: power spectrum

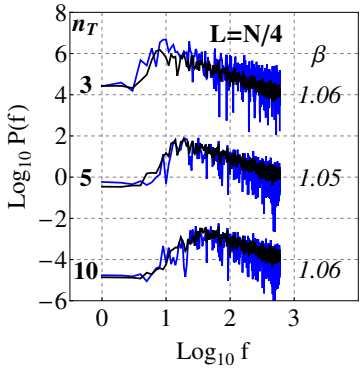

(1b) TBRE ensemble: power spectrum

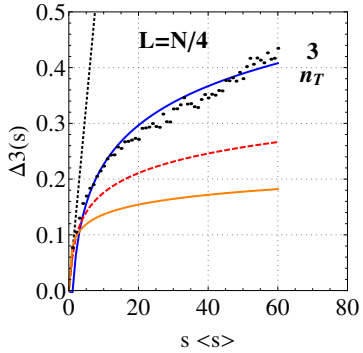

(2a) Realistic calculation: Δ_3

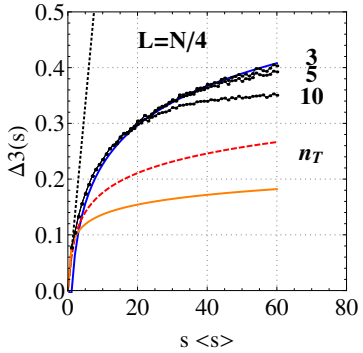

(2b) TBRE ensemble: Δ_3

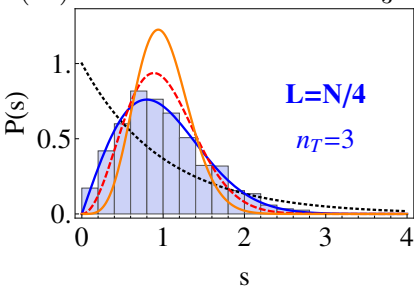

(3a) Realistic calculation: NNS

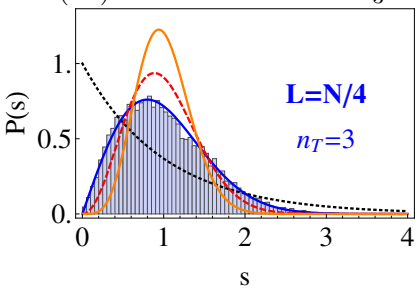

(3b) TBRE ensemble: NNS

Figure 4. Fluctuation measures for the theoretical $J^\pi = 4^+$ subspectrum of ^{48}Ca, for a single realization using a realistic interaction (left panels (a)) and a Two-Body Random Ensemble (TBRE) (right panels (b)). (Upper row (1)) The Fourier power spectrum $P(f)$ for the detrended fluctuation series $\widetilde{E}(i)$ of eq. (7) follows a power law $P(f) \sim 1/f^\beta$ with $\beta \approx \gamma \approx 1$. Shown for embedding dimension $L = N/4$ and for number of trend components $n_T \geq 3$. The power law is independent from the particular choice of the parameters L and n_T. Shown for a single realization of the spectrum (blue), and for an ensemble mean (black). (Middle panels (2)) The long-range fluctuation measure Δ_3 for the detrended and rescaled energies $\eta(i)$ of eq. (8) corresponds with the GOE prediction (blue, continuous line), compared with predictions for the Poisson (black, dotted line), GUE (red, dashed line) and GSE (orange, continuous line) cases. Shown for embedding dimension $L = N/4$ and number of trend components $n_T = 3, 5$ and 10. (Bottom panels (3)) The short-range fluctuation measure of the Nearest-Neighbour Spacing (NNS) distribution for the detrended and rescaled level spacings $s(i) = \eta(i) - \eta(i-1)$ of eq. (10) corresponds with the GOE prediction (blue, continuous line), compared with predictions for the Poisson (black, dotted line), GUE (red, dashed line) and GSE (orange, continuous line) cases. Shown for embedding dimension $L = N/4$ and number of trend components $n_T = 3$. The results are independent from the embedding dimension L and the number of trend components n_T. It can be appreciated that the level spacings s have been normalized to $\langle s \rangle = 1$.

References

[1] Berry M V and Tabor M 1977 *Proc. Roy. Soc. A* **356** 375
[2] Bohigas O, Giannoni M J and Schmit C 1984 *Phys. Rev. Lett.* **52** 1
[3] Mehta M L 1991 *Random Matrices* 2nd ed. (New York: Acad. Press)
[4] Relaño A, Gómez J M G, Molina R A, Retamosa J and Faleiro E 2002 *Phys. Rev. Lett.* **89** 244102
[5] Kota V B K 2001 *Phys. Rep.* **347** 223
[6] Papenbrock T and Weidenmüller H A 2007 *Rev. Mod. Phys.* **79** 997
[7] Weidenmüller H A and Mitchell 2009 G E *Rev. Mod. Phys.* **81** 539
[8] Guhr T, Müller-Groeling A and Weidenmüller H A 1998 *Phys. Rep.* **299** 189
[9] Haake F 2010 *Quantum signatures of chaos* 3rd ed. (Heidelberg: Springer)
[10] Gómez J M G, Kar K, Kota V B K, Molina R A, Relaño A and Retamosa J 2011 *Phys. Rep.* **499** 103
[11] Zelevinsky V 2001 *Phys. E* **9** 450.
[12] Brody T A, Flores J, French J B et al. 1981 *Rev. Mod. Phys.* **53** 385
[13] Shukla P 2012 *Int. J. Mod. Phys. B* **26** 1230008
[14] Gómez J M G, Molina R A, Relaño A and Retamosa J 2002 *Phys. Rev. E* **66** 036209
[15] Bae M S, Otsuka T, Mizusaki T and Fukunishi N 1992 *Phys. Rev. Lett.* **69** 2349
[16] Enders J, Guhr T, Heine A et al. 2004 *Nucl. Phys. A* **741** 3
[17] Fossion R and Bijker R 2009 *Rev. Mex. Fís.* S **55** 41
[18] Landa E, Morales I O, Hernández C, López Vieyra J C and Frank A 2008 *Rev. Mex. Fís.* S **54** 48
[19] Jackson A D, Mejia-Monasterio C, Rupp T, Saltzer M and Wilke T2001 *Nucl. Phys. A* **687** 405
[20] Gómez J M G, Relaño A, Faleiro E et al. 2005 *Phys. Rev. Lett.* **94** 084101
[21] Relaño A, Molina R A and Retamosa J 2004 *Phys. Rev. E* **70** 017201
[22] Landa E, Morales I O, Fossion R et al. 2011 *Phys. Rev. E* **84** 016224
[23] Morales I O, Landa E, Stránský P and Frank A 2011 *Phys. Rev. E* **84** 016203
[24] Wu Z, Huang N E, Long S R and Peng Ch-K 2007 *Proc. Nat. Acad. Sci.* **104** 14889
[25] Elsner J B and Tsonis A A 1996 *Singular Spectrum Analysis:* (New York: Plenum Press,)
[26] Golyandina N et al. 2001, *Analysis of time series structure* (London: Chapman & Hall/CRC).
[27] Alexandrov T, Bianconcini S, Dagum E B, Maass P and McElroy T 2012 *Econometric Rev.* **31** 593
[28] Gao J B, Cao Y and Lee J M 2003 *Phys. Lett. A* **314** 392
[29] Santhanam M S, Bandyopadhyay J N and Angom D 2006 *Phys. Rev. E* **73** 015201(R)
[30] Gómez J M G et al. 1998 *Phys. Rev. C* **58** 2108.
[31] Caurier E , J.M.G. Gómez, V.R. Manfredi and L. Salasnich et al. 1996 *Phys. Lett. B* **365** 7
[32] Caurier E and Nowacki F 1989 code Antoine, Strasbourg
[33] Kuo T et al. 1968 *Nucl. Phys. A* **114** 241.
[34] Poves A et al. 1981 *Phys. Rep.* **70** 235
[35] Flores J, Horoi M, Müller M and Seligman T H 2001 *Phys Rev E* **63** 026204
[36] Bethe H A 1936 *Phys. Rev.* **50** 332
[37] Zuker A P 2001 *Phys. Rev. C* **64** 021303
[38] Dean D J, Koonin S E, Langanke K, Radha P B and Alhassid Y 1995 *Phys. Rev. Lett.* **74** 2909
[39] Fossion R, Torres Vargas G, Velázquez V and López Vieyra J C, in preparation